Size Effects on Photodissociation and Caging of Hydrogen Bromide Inside or on the Surface of Large Inert Clusters: From One to Three Icosahedral Argon Layers

Petr Slavíček, Petra Žďánská, and Pavel Jungwirth*

J. Heyrovský Institute of Physical Chemistry, Academy of Sciences of the Czech Republic, Dolejškova 3, 18223 Prague 8, Czech Republic

Reinhard Baumfalk and Udo Buck

Max-Planck-Institut für Strömungsforschung, Bunsenstrasse 10, 37073 Göttingen, Germany

Received: March 31, 2000; In Final Form: May 25, 2000

Molecular dynamics simulations have been employed for the study of photolysis of hydrogen bromide placed inside or on the surface of Ar_{12}, Ar_{54}, Ar_{97}, and Ar_{146} clusters, representing one to three icosahedral solvation shells. A large set of classical Wigner trajectories, which take into account the initial quantum rotational or librational delocalization of HBr, is generated and analyzed in terms of transient hydrogen populations inside the cluster and final kinetic energy distributions. The key result is that for fully solvated HBr the size effect on caging is dramatic in the studied range of cluster sizes, while it is only moderate for surface isomers. Simulations also demonstrate that caging can be efficiently turned off by a librational preexcitation of HBr on argon clusters. Calculations are compared to results of cluster experiments which have measured the kinetic energy distribution of hydrogens originating from HBr photolysis at 243 nm in or on argon clusters with an average size of 115 atoms, and a near-quantitative agreement is found.

I. Introduction

The cage effect, which is the ability of a solvent to hinder photodissociation of a solvated chromophore and possibly to cause recombination, was originally described in the condensed phase.[1,2] Recently, this effect has been also intensely studied in finite size clusters ranging from a single solvent atom to systems with tens to hundreds of atoms. New phenomena, that appear in clusters and are not present in the bulk liquid or solid, are connected with the large surface of the clusters and with the fact that the systems are prepared under cryogenic conditions. Namely, the former feature leads to the fact that caging can strongly depend on the solvation site and the resulting photodissociation process will be different for surface vs fully solvated chromophores. Very low temperatures reached when clusters are prepared by supersonic jet expansion into a vacuum amplify the importance of quantum vibrational and rotational effects, especially if hydrogen is one of the potential photoproducts.

Rare gas clusters with a hydrogen halide chromophore have served as prototypical systems for the computational study of the cage effect. A significant effort has been directed to the investigation of the single atom cage effect in Ar−HCl and Ar−HBr clusters.[3−6] Although the optimal geometry of these clusters is collinear, due to a large librational (bending) delocalization of the hydrogen, caging is extremely inefficient in these small clusters.[4]

In the past decade, a considerable theoretical effort has been devoted to the study of larger $HX(Ar)_n$ (X = F,Cl,Br and n = 2−54) clusters having up to two icosehadral rare gas solvation shells.[7−14] The gradual emergence of efficient caging upon increasing the cluster size has been investigated both for the fully solvated HX molecule and for the chromophore placed on the surface of the cluster. Various levels of theoretical description of both the initial vibrational/rotational state of the complex and of the photodissociation dynamics have been employed. It has been shown that hydrogen is strongly delocalized in the angular coordinates and that it is important to correctly describe the initial quantum librational or rotational state of the hydrogen halide.[13,14] For the photodissociation dynamics involving a highly energetic hydrogen, quantum effects are less important. Unless one is interested in subtle details such as interferences and vibrational resonances,[13,14] the process can be reasonably described using Wigner trajectories.[9−11,15] Finally, we note that the products of photolysis correspond to different spin−orbit states of the halogen atom. Especially for heavier halogens, it is important to take into account spin−orbit interactions and possibly also nonadiabatic transitions between low-lying excited states of the system.[9−11]

Experiments for larger clusters than 1:1 complexes are still rare. One measurement has been carried out for neat $(HBr)_n$ clusters for sizes up to $\bar{n} = 10$.[16] Very recently the kinetic energy distributions of the H atom products of photodissociated HBr molecules embedded in or adsorbed on large Ar_n clusters of the average size $\bar{n}$ = 115−139 has been measured.[11] So far, the data could only be compared with calculations for $HCl(Ar)_n$ with sizes up to $n = 55$.[11] The main goal of this work is to present both simulations and experiments of HBr photodissociation and caging in and on large argon clusters and to investigate the size effect from one to three icosahedral argon layers. The paper presents the first direct comparison between calculation and experiment for large $HBr(Ar)_n$ clusters and for the first time theoretically addresses hydrogen halides with more than two rare gas solvation layers. The results are analyzed and compared primarily in terms of the kinetic energy distributions of the outgoing hydrogen, which directly reflect the caging process. Simulations allow us also to quantify the cage effect in terms of survival probabilities, i.e., transient probabilities of

10.1021/jp001262q CCC: $19.00
Published on Web 07/21/2000

finding the photolyzed hydrogen inside the cage. A novel way of controlling the efficiency of the cage effect for surface structures is demonstrated in the calculations. Namely, caging can be turned off by a librational excitation of the HBr molecule prior to the UV photolysis.

The rest of the paper is organized as follows. Systems and potentials are briefly described in Section II. Computational methods are presented in Section III and the experimental details in Section IV. Section V contains the results and discussion and concluding remarks are given in Section VI.

II. Systems and Potentials

A. Geometry. It is well-known both from theory and experiment that argon clusters up to about a thousand atoms prefer icosahedral geometry.[17,18] Geometry and symmetry of larger argon clusters is only slightly perturbed by the presence of a hydrogen halide molecule.[19] In this study, we investigate $HBr(Ar)_{12}$, $HBr(Ar)_{54}$, $HBr(Ar)_{146}$, and $HBr(Ar)_{97}$ clusters. The first three clusters correspond to one to three complete icosahedral layers, the last system is a cluster with a half-filled third solvation layer. For each cluster size we have assumed two structures: An embedded isomer with HBr in the central position of cluster and a surface isomer with HBr on the cluster surface in the vertex of the icosahedral structure. Note that both embedded and surface solvated hydrogen halides are stable under experimental conditions.[19] The HBr molecule in these clusters is assumed to occupy a substitutional position replacing a single argon atom. This choice is natural for embedded $HBr(Ar)_n$ isomers, while for surface isomers, structures where HBr is simply added to the surface of an argon cluster are also plausible.[11] However, for magic number argon clusters with complete solvation shells, structures with HBr in a substitutional position are more stable. While in the embedded isomers, hydrogen almost freely rotates even in the ground rotational state, for the surface isomers the motion of the light atom is more hindered and hydrogen librates.[13,14] Optimized structures have been obtained by energy minimizations started from ideal geometries of unperturbed argon clusters, taking into account the rotational or librational state of the hydrogen halide.[13,14]

B. Potentials. Interactions in the ground electronic state of $HBr(Ar)_n$ are approximated by a three-body potential for Ar−HBr[20] and by pair potentials for the remaining parts. For the argon−argon interaction we have adopted the potential by Aziz and Slaman.[21] The bonding interaction between hydrogen and bromine is approximated by a harmonic potential.[22]

For low-lying electronically excited states, the potential is constructed using a Diatomics-in-Molecule Hamiltonian, in which the anisotropy of the bromine−argon interaction is explicitly taken into account.[23] The argon−argon interaction is assumed to be the same as that in ground electronic state. The mostly repulsive argon−hydrogen potential, the slope of which strongly influences the efficiency of caging, is taken from accurate ab initio calculations.[13] In the course of HBr photodissociation two electronic states play a dominant role: The $^1\Pi_1$ state, which correlates with the ground H + Br asymptote, and the $^3\Pi_0$ state, which corresponds to the spin-orbitally excited H + Br* dissociation channel. The potentials for these states have been adopted from a previous work by Pouilly et al.[24] In the region of 243 nm photoexcitation from the ground state and for larger internuclear separations the present H−Br potentials are practically identical to those used in older calculations by Guo et al.[25]

III. Computational Methods

A. Initial State. Under experimental conditions, corresponding to a supersonic jet expansion into the vacuum, the nascent clusters possess very low temperatures, typically from several to few tens of Kelvins. For this reason, quantum effects can play an important role (especially if hydrogen is present in the system) and an accurate knowledge of the initial vibrational/rotational wave function is needed for a quantitative understanding of the subsequent photodissociation process. In this study, the following approach to the construction of the initial wave function is adopted. The hydrogen and cage modes, as well as HBr rotation (libration) and vibration, are assumed to be decoupled. Such an assumption is plausible at low cluster temperatures present in the experiment. For HBr vibration and for the cage modes, the initial state can be treated within the harmonic approximation, however, the HBr rotational (librational) motion should be described more accurately.[13,14]

The initial wave function Ψ_0 is then expressed as:

$$\Psi_0(q_1, ..., q_{3n-3}, \rho, \phi, \theta) \propto e^{(-1/2\omega_1 q_1^2)} ... e^{(-1/2\omega_{3n-3} q_{3n-3}^2)} \frac{\chi(\rho)}{\rho} \Phi(\phi,\theta) \quad (1)$$

where q_i are the normal coordinates of the cage (by cage we understand here all the heavy atoms), ρ, ϕ, and θ are spherical coordinates of the HBr molecule, ω_i are the vibrational frequencies of the cage modes, and n is the number of argon atoms. Finally, χ is the (harmonic) H−Br vibrational function, and the factor $1/\rho$ comes from the use of spherical coordinates. The initial rotational (librational) wave function Φ of the HBr molecule corresponds either to the lowest or to excited states. These states have been obtained using a truncated expansion in the basis of spherical harmonics.[13] The corresponding Hamiltonian describes the rotation (libration) of HBr in the potential caused by the cage atoms. This effective potential depends on the optimal cluster geometry, which in turn depends on the initial rotational (librational) function. Thus, the wave function and the equilibrium geometry are calculated in a self-consistent way.[13,14]

B. Wigner Trajectories. While the initial state of the cluster is strongly quantum mechanical, the importance of quantum effects decreases upon photoexcitation, which pumps more than an electronvolt of excess energy into the system. Here, we have adopted an approach based on Wigner trajectories for the description of the photodissociation process. Within this method, the initial positions and momenta for a set of classical trajectories are obtained using a Wigner mapping of the initial wave function.[15] In this way, the quantum nature of the initial state is taken into account. The Wigner transformation of a harmonic wave function is known analytically, and the transformations for rotational (librational) wave functions have been calculated numerically.[13,14] Direct application of the Wigner transformation provides an adequate set of initial coordinates and momenta corresponding to a vertical excitation (e.g., using an ultrashort laser pulse). Since here we are modeling an experiment which employs excitation light with a fixed wavelength, the initial conditions should be filtered to satisfy the relation:

$$E_{exc} = \hbar\omega - D_0 + E^e_{Ar-HBr} - E^g_{Ar-HBr} \quad (2)$$

where $\hbar\omega$ is the energy of the exciting photon, D_0 is the dissociation energy of the H−Br bond, E_{exc} is the excess energy of the H + Br photofragment, and E^g_{Ar-HBr} and E^e_{Ar-HBr} are the interaction energies between argons and HBr in the ground

and in the excited states. We have carried out the energy filtering in the following way. First we have sampled the initial rotational (librational) wave function and the cage modes. In a second step we have prolonged the H−Br bond to a distance where relation 2 is satisfied. Such a procedure is justified by the fact that the energy of the system dominantly depends on the H−Br distance, while it is rather insensitive to HBr rotation or libration and, within certain margins, also to cage motions. In our simulations we have chosen the excitation energy to be 5.08 eV, which corresponds to the experimental wavelength of 243 nm. It has already been mentioned that the post excitation dynamics takes place primarily on two electronic potential surfaces, which correspond to the $^1\Pi_1$ and $^3\Pi_0$ states of HBr. The region to which the HBr molecule is promoted by the 243 nm radiation is close to the crossing between these two curves and the dissociating hydrogen is unlikely to return there. As a result, the Br*/Br branching ratio in rare gas clusters will not differ significantly from the gas-phase value. This has been confirmed in recent experiments on neat $(HBr)_n$ clusters, which give a value of 0.2 for this branching ratio.[16] Wigner trajectories have been propagated on both excited surfaces and measurable quantities have been weighted by this ratio. 700 Wigner trajectories have provided converged results. The total simulation time has been 1.5 ps with a time step of 0.0241 fs.

The positively definite Wigner distribution for the ground rotational (librational) state can be directly used as a probability function. Since we have also studied the influence of IR preexcitation on photodissociation dynamics of surface solvated HBr, sampling of higher librational states is needed, too. For these states the Wigner quasi-probability becomes oscillatory and is no more positively definite, therefore, it is computationally difficult to sample it by a sufficient number of trajectories. For this reason, excited-state librational wave functions have not been sampled using Wigner distribution but via the square of the wave function in the usual coordinate representation,[26] similarly as in our previous work.[13,14] The corresponding classical momenta, which are typically small for low-lying librational states, are then chosen simply to satisfy the condition of correct quantum librational energy.[13,14] Although the trajectories originating from excited librational states are then not truly Wigner trajectories, the shape of the initial wave function in the coordinate space is now properly sampled, which is crucial for a correct description of the librational control of the photodissociation and of the caging process.[13]

C. Quantum Dynamics. For comparison, we have also performed a quantum dynamical simulation for the smallest $HBr(Ar)_{12}$ cluster, corresponding to a vertical excitation by an infinitely short optical pulse. A numerically exact quantum simulation in full dimensionality for the system under study is computationally infeasible. Since the cage atoms are relatively heavy, the most important quantum effects are connected with the hydrogen motion. For this reason, the hydrogen atom has been treated properly as a quantum particle, while the motion of the remaining atoms has been described using Wigner trajectories. The interaction between the cage and the hydrogen atom is taken into account within the mean field Classical Separable Potential (CSP) method.[27]

The computational implementation of the quantum dynamical method has been presented in considerable detail in our previous studies;[13,14] here we provide only the most important facts. The hydrogen wave function has been discretized on a 3D Cartesian grid. For the description of the wave function inside the cluster area $200 \times 200 \times 200$ grid points have been employed. Outside the cluster a cubic imaginary potential has been added in order to absorb the outgoing part of the wave function. For the construction of the CSP potential 150 Wigner trajectories have been employed. To preserve the symmetry of the $HBr(Ar)_{12}$ the initial conditions for the Wigner trajectories have been subsequently symmetrized. A split operator method[28] with a time step of 0.0241 fs has been employed for the quantum propagation on the excited potential surface corresponding to the $^1\Pi_1$ state of HBr.

IV. Experimental Procedures

The experimental setup used in the photodissociation measurements is based on the molecular beam machine and the laser system which are described in detail elsewhere.[29,30] Here, only a very short summary of the major components is given including the implemented experimental improvements.[16] The cluster beams are produced by a supersonic expansion of the neat argon gas or a mixture of a small amount of HBr in argon into the source chamber through a nozzle of conical shape with a diameter of $d = 60\ \mu$m, an opening angle of 30° and a length of 2 mm. A typical pressure is 3.8 bar. The size of the argon clusters is determined by changing the source temperature. At a temperature of 229 K the average cluster size is $\bar{n} = 115$.[31]

After passing several differentially pumped vacuum chambers, the molecular beam enters the detection chamber hosting a two-stage time-of-flight mass spectrometer (TOFMS) of the Wiley−McLaren type. It is surrounded by a copper shield mounted on a high-pressure helium compressor which keeps the temperature at 20 K. To dissociate the clusters, polarized laser light is focused into the mass spectrometer by a 400 mm lens. At this interaction point, the molecular beam, the dissociation laser beam, and the TOFMS collection axis are oriented mutually perpendicular to each other. Thus, Doppler effects are eliminated in the photodissociation measurements.

For ionization, the same experimental arrangement as for the dissociation is used. At 243.06 nm, dissociation and ionization take place within the same laser pulse. The detection of H fragments occurs by one-color, resonance enhanced multiphoton ionization (REMPI) in a (2+1) excitation scheme. The 243.06 nm light is generated by mixing the fundamental of an injection seeded Nd:YAG laser (Quanta Ray GCR-5) with the frequency doubled output of a dye laser (LAS, LDL 20 505) operating at 630.3 nm and pumped by the second harmonic of the Nd:YAG laser at 532 nm.

The preparation of the HBr molecule on the surface or inside the argon cluster is crucial for the present experiment. Therefore this part was carried out quite carefully.[11] For the surface case, the pick-up technique was used. The argon clusters pass a scattering cell filled with HBr gas. The pressure of this gas is adjusted in such a way that mainly HBr monomers are captured by the argon clusters. The molecules do not penetrate inside the cluster, since the surface position is the global minimum of the potential surface and the cluster is solid. To reach the inside configuration, HBr gas was expanded adiabatically together with argon into a supersonic nozzle beam. In this case the problem is to avoid the formation of HBr clusters. The solution is to go to very dilute mixtures. A 0.1% mixture at low temperatures allowed us to generate the required configuration, a single HBr molecule embedded in an argon cluster of the average size $\bar{n} = 115$.[11]

The observable data discussed in the present paper is the kinetic energy of the outgoing hydrogen atoms. It is obtained from a careful analysis of the measured time-of-flight spectra in the TOFMS which is operated in the so-called low field mode. In this way also particles with zero velocities are detected. The

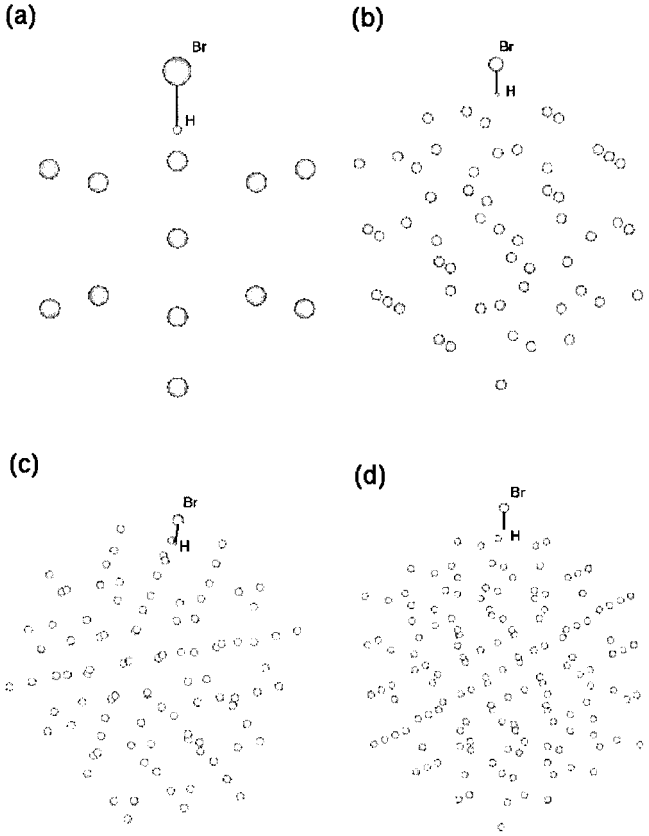

Figure 1. Geometries of the surface isomers of the (a) $HBr(Ar)_{12}$, (b) $HBr(Ar)_{54}$, (c) $HBr(Ar)_{97}$, and (d) $HBr(Ar)_{146}$ clusters.

transformation from time to energy variables is carried out by a complete simulation of the particle trajectories taking into account the photodissociation process, the molecular beam data, the finite interaction volume, and the detector dimensions. In this way the excess energy of the system is reflected in the kinetic energy of the H atom. The direct cage exit leaving the Br atom in two spin−orbit states is given by 1.36 and 0.89 eV at the wavelength of 243 nm, while completely caged H atoms appear at zero kinetic energy.

V. Results and Discussion

A. Systems. Optimal structures of $HBr(Ar)_n$ (n =12, 54, 97, and 146) clusters are depicted in Figure 1. Only the surface isomers are shown. The embedded HBr molecule is difficult to display for large clusters, moreover the argon structures are very similar for both isomers. In case of a complete first, second, or third solvation shell the embedded isomers preserve the icosahedral geometry of the corresponding magic number argon cluster, while this symmetry is marginally distorted for the surface isomers. The symmetry of the $HBr(Ar)_{97}$ cluster with a half-filled third solvation layer is lower.[32] Both embedded and surface structures considered in the present calculations represent energetically favorable isomers, which are experimentally relevant. However, it should be mentioned that clusters prepared by supersonic jet expansion have a distribution of sizes and the rapid cooling process can lead to an occurrence of also energetically higher isomers in the cluster beam.

Hydrogens, depicted in Figure 1, represent the mean positions for ground HBr librational states. In fact, hydrogen undergoes large amplitude motions, librating for the surface isomers and almost freely rotating for the embedded structures.[13,14] Figure 2 shows the initial ground and excited librational wave function for the surface isomer of $HBr(Ar)_{12}$. These wave functions are

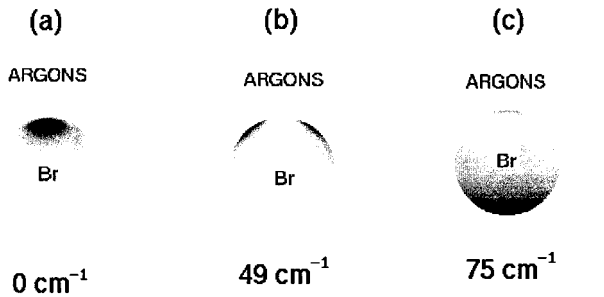

Figure 2. Librational wave functions for the HBr surface solvated on the Ar_{12} cluster, corresponding to the (a) ground, (b) first (doubly degenerate) excited, and (c) first nondegenerate exited state. The energies are relative to the ground librational state.

practically the same for all cluster sizes under study. The ground rotational wave function for the embedded isomers, which corresponds to an almost free rotor,[13] is totally structureless and is not shown here. In Figure 2, the high density of dots corresponds to high hydrogen probability, while low density means low probability or nodes on the librational wave function. Figure 2a depicts the ground librational state, Figure 2b the doubly degenerate first excited state, and Figure 2c the first nondegenerate excited librational state. The optimal positions of heavy atoms are almost constant for different librational states, whereas the shapes of the librational wave functions change dramatically. While in the ground-state hydrogen points toward the cluster, low-lying excited librational states correspond to hydrogen directed mostly sidewise or away from the argon atoms. As discussed below, this has a pronounced effect on the subsequent photodissociation and caging. The librational excitation energies lie between 50 and 75 cm^{-1} for the lowest excited states corresponding to librational temperatures of 70−100 K. As a consequence, for temperatures of a few tens of Kelvins assumed for the clusters after supersonic expansion, predominantly the ground librational state should be populated.

B. Calculated Survival Probabilities and KED Spectra. Photodissociation dynamics following the excitation of the HBr molecule by a 243 nm radiation has been simulated using the Wigner trajectories approach. The main focus of the present study has been the effect of caging by rare gas atoms. In particular, we have investigated how caging depends on cluster size, the effect of different isomeric structures (surface vs embedded HBr), and also the effect of the initial librational state on caging.

One way to quantify the cage effect is to evaluate the survival probabilities, i.e., the transient probabilities of finding the photodissociating hydrogen inside the cluster. Figure 3 (Figure 4) depicts these survival probabilities for embedded (surface) isomers of different sizes initially in the ground rotational (librational) state of HBr. There is a dramatic difference in the decay of the hydrogen population in the cage between the two smaller and the larger clusters with embedded HBr. Figure 3 clearly shows that the first two solvation layers are quite inefficient in caging, which only becomes strong after the third argon layer starts to build up. The size dependence is much weaker for surface isomers where we see a continuous increase of the transient survival probabilities upon enlarging the cluster.

A quantity which allows us to perform a direct comparison with experiment is the final kinetic energy distribution (KED) of the outgoing hydrogen. The KED spectra in the present simulations have been obtained by making a histogram of the hydrogen kinetic energy at a time when hydrogen is already outside the cage for all Wigner trajectories. KED spectra for $HBr(Ar)_{12}$, $HBr(Ar)_{54}$, $HBr(Ar)_{97}$, and $HBrAr_{146}$ are depicted

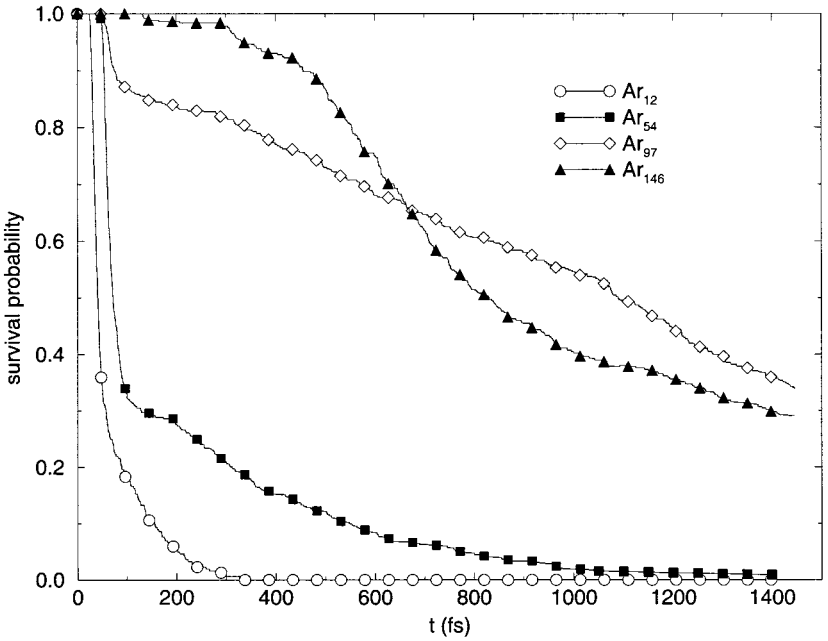

Figure 3. Transient probabilities of finding the photodissociating hydrogen inside the cluster for embedded HBr(Ar)$_n$ ($n = 12-146$) isomers.

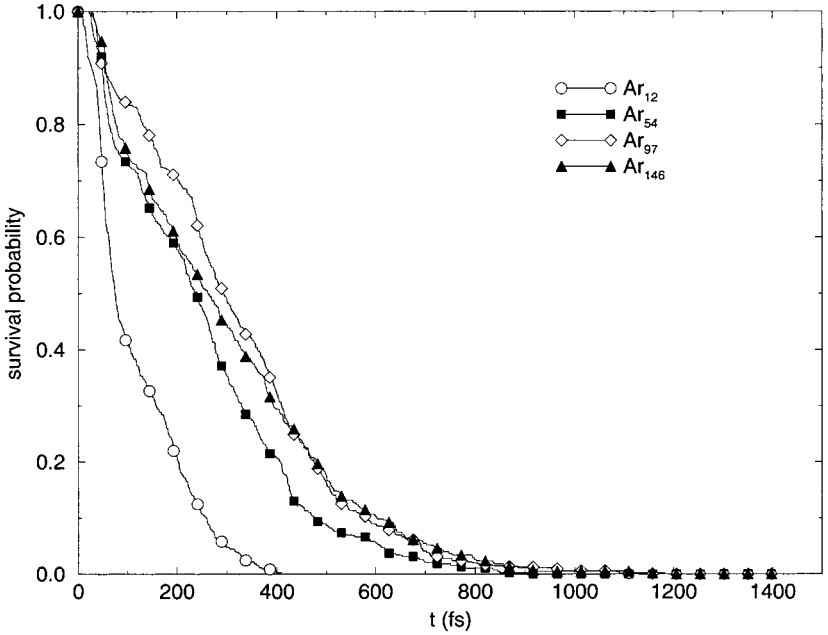

Figure 4. Transient probabilities of finding the photodissociating hydrogen inside the cluster for surface solvated HBr(Ar)$_n$ ($n = 12-146$) isomers.

in Figures 5−8. For each cluster size two KED spectra have been evaluated, corresponding to the embedded or surface isomer. The KED spectra for these two isomers differ significantly from each other at each size. Note, that caging is very inefficient for the embedded isomer of HBr(Ar)$_{12}$. As a result, high energy peaks at 1.3 and 0.9 eV, corresponding to directly exiting hydrogens for the Br and Br* channels, represent the main features in the KED. Upon adding more argon atoms, a peak at zero hydrogen velocity, which corresponds to efficient caging, starts to grow and finally dominates the spectrum. For large embedded isomers, we see only a small component of fast hydrogen for the HBr(Ar)$_{97}$ cluster with a half-filled third solvation layer and zero intensity at high kinetic energies for the HBr(Ar)$_{146}$ cluster with three complete solvation layers. In contrast, the KEDs for surface isomers change only slightly upon increasing the cluster size from 12 to 146 argon atoms. Even for the smallest surface isomer under study, the HBr(Ar)$_{12}$ cluster, caging is efficient and, consequently, a significant signal at zero kinetic energy is observed. The results for the three larger surface isomers are very similar. The dominant signal appears at zero velocity, however, the fast hydrogen component does not vanish even for the largest cluster. Effectively, HBr deposited on the argon cluster surface is surrounded by more argon solvation layers, than for the embedded isomer of the same size. On the other hand, some trajectories corresponding to tails of the librational wave functions do not penetrate into the argon cluster. This behavior is responsible for the occurrence of the high energy peaks on KEDs for surface isomers. This fraction of trajectories is practically independent of cluster size in the studied range.

C. Comparison with Experimental KED Spectra. The experimentally measured kinetic energy distributions of the photolyzed hydrogen for large HBr(Ar)$_n$ clusters are depicted in Figure 9. Figure 9a shows the result for the embedded isomer,

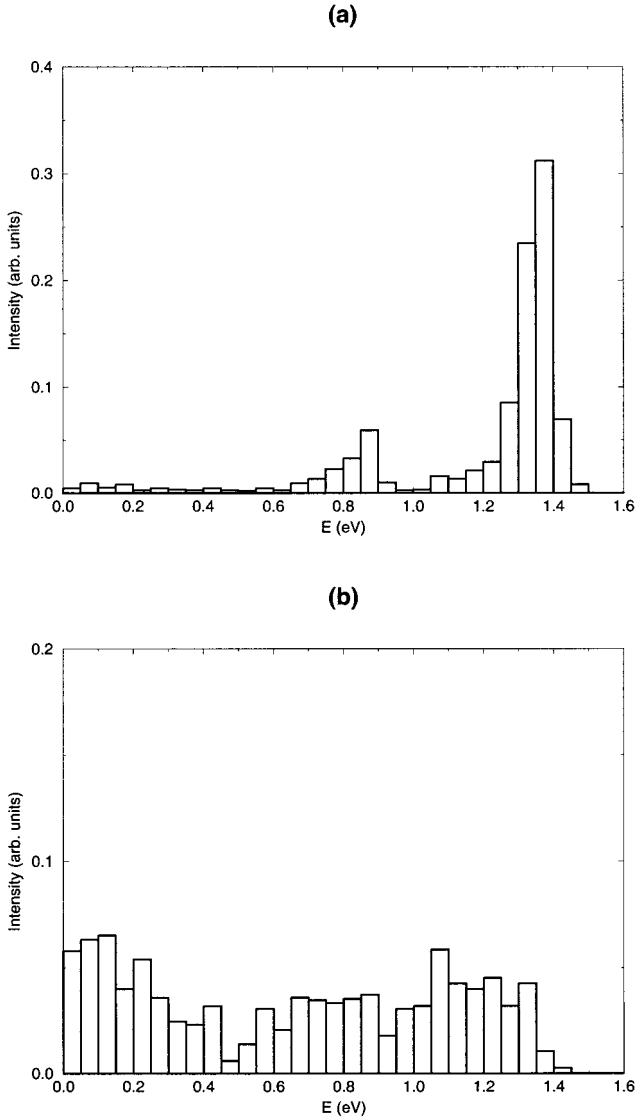

Figure 5. Final kinetic energy distributions of the photolyzed hydrogen for the (a) embedded and (b) surface isomers of $HBr(Ar)_{12}$.

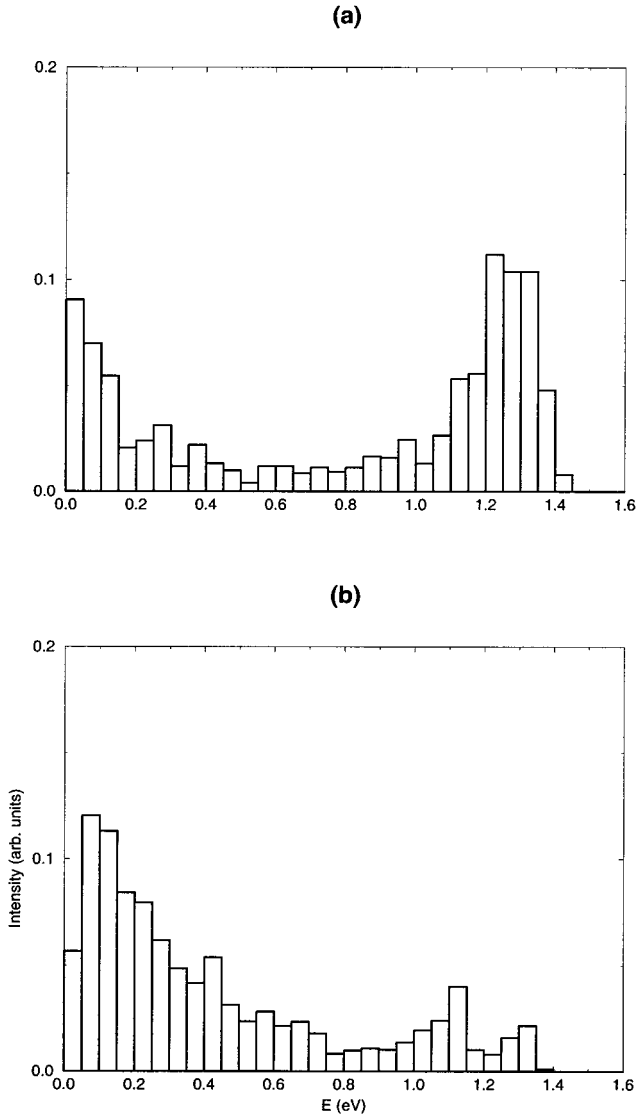

Figure 6. Final kinetic energy distributions of the photolyzed hydrogen for the (a) embedded and (b) surface isomers of $HBr(Ar)_{54}$.

while Figure 9b presents that for the surface structure. The mean number of argon atoms solvating HBr is 115 in both cases. Both for the embedded and surface isomers, the zero velocity peak is dominant. For the surface isomer, a significant peak around 1.2−1.3 eV and a smaller one at 0.8 to 0.9 eV are also observed. They are an indication of a direct cage exit of the hydrogen atoms reflecting the populations of the two spin−orbit states of Br. For the embedded case, the peak at zero energy is much larger than that at 1.3 eV, also in contrast to the surface case.

The experimental results can be readily compared with simulations of $HBr(Ar)_{54}$ to $HBr(Ar)_{146}$ clusters depicted at Figures 6 to 8. For the embedded case, it is quite obvious that the calculation for $HBr(Ar)_{97}$ has the closest resemblence to the experimental result. In this case only, we observe a large peak at zero velocity and a small peak at 1.3 eV, the indications of both caging and the cage exit. For the other two cluster sizes, either the large peak at 1.3 eV (see Figure 6) or the peak at zero energy (see Figure 8) predominate. The direct comparison between the simulation for $HBr(Ar)_{97}$ and experiment shows a near-quantitative agreement, the peak intensities included. There is only a small discrepancy in the missing intensity between 0.4 and 1.0 eV, which is discussed below. Similar considerations hold also for the surface case, although now the calculated spectra are much more similar for different cluster sizes. Nevertheless, the agreement between experiment and theory is again best for the simulated $HBr(Ar)_{97}$ cluster, where the structure of the two high energy peaks is most satisfactorily reproduced. Small discrepancies occur in the ratio of the intensities at zero energy and at 1.3 eV (vide infra).

Note that the experiment generates clusters with a certain size distribution. This can explain small differences between experiment and simulation in the sharpness of the peaks in the KED spectra, especially for the embedded case. The calculated KEDs for $HBr(Ar)_{59}$ exhibit intensities in the 0.4−1.0 eV range, which are lacking in the calculated $HBr(Ar)_{97}$ case. Therefore, contributions from smaller clusters which are present in the experiment might well explain the small deviations. For surface isomers, only a weak size dependence of the KED spectra is observed. Here, another rationalization of the minor difference between experiment and simulation should be invoked, namely that the experimental structures for a given cluster size are probably not unique. As discussed above, in the calculations we have considered surface structures in which the HBr molecule replaces one argon from the last solvation shell. Another possibility is to deposit HBr on the surface of a cluster, e.g., with all solvation layers filled, instead of replacing one of the argon atoms. Such structures might also contribute to the

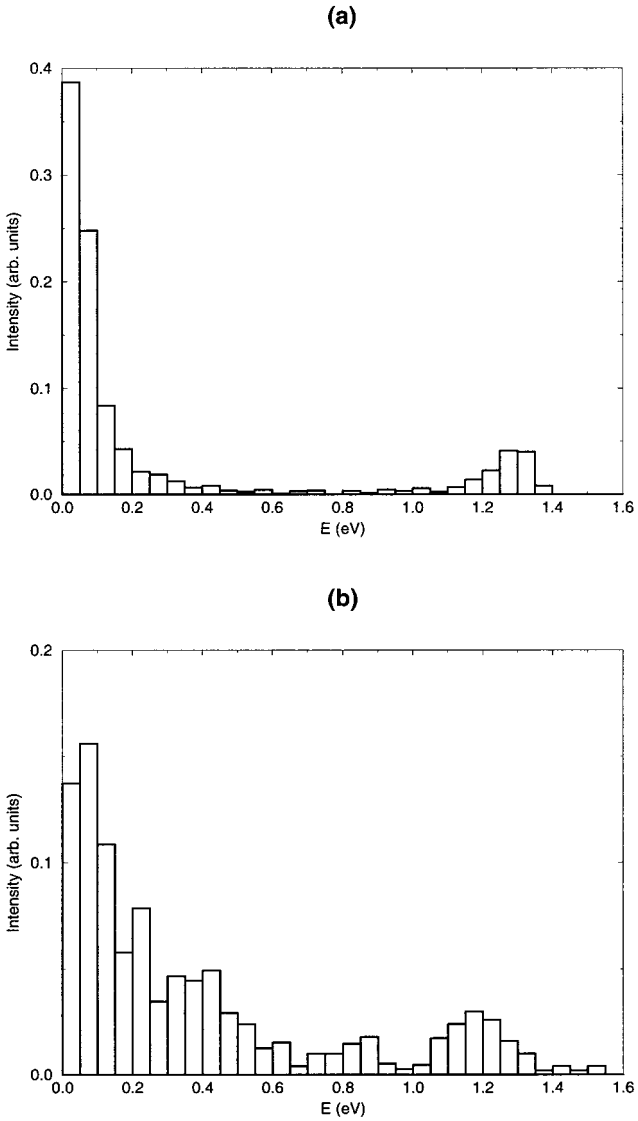

Figure 7. Final kinetic energy distributions of the photolyzed hydrogen for the (a) embedded and (b) surface isomers of $HBr(Ar)_{97}$.

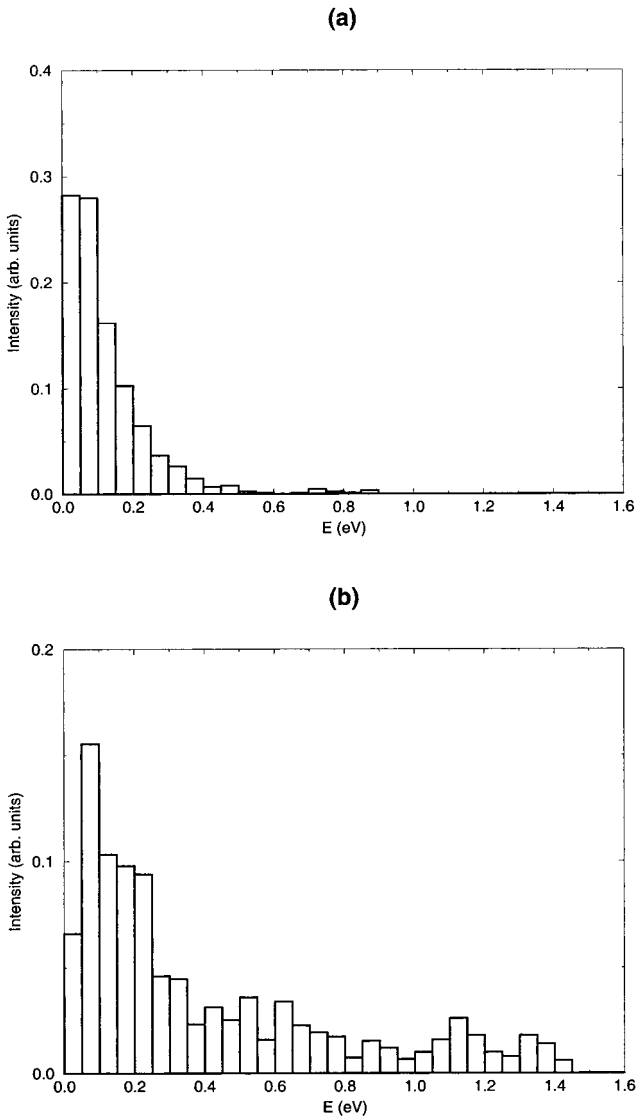

Figure 8. Final kinetic energy distributions of the photolyzed hydrogen for the (a) embedded and (b) surface isomers of $HBr(Ar)_{146}$.

experimental signal.[11] Present calculations show that in such cases the component corresponding to fast hydrogen becomes more important, which may explain the slightly different experimental and calculated intensities of the high energy peaks for surface isomers. Finally, preliminary measurements on clusters with varying numbers of argon atoms[33] confirm very well the trends emerging from the present calculations on clusters with one to three solvation layers. We can conclude that the good agreement between theory and experiment for both embedded and surface isomers not only indicates the quantitative predictive power of the calculations, but also confirms that the experimental concepts for the production of these species are quite reliable.

D. Librational Control. Photodissociation dynamics and caging of HBr deposited on argon clusters strongly depends on the initial librational state. We demonstrate this librational control mechanism[14,34,35] on the largest $HBr(Ar)_{146}$ cluster, where the influence of the initial librational state is the strongest. However, qualitatively the same effect is present for all surface structures.

The effect of librational excitation prior to the 243 nm photolysis is clearly seen on time evolution of transient probabilities of finding hydrogen inside the cluster. Figure 10 depicts these survival probabilities for the ground, the degenerate first excited, and the first nondegenerate excited librational state. The differences in the transient survival probabilities are remarkable, especially between the ground and first nondegenerate excited librational states. While for the case of photodissociation from the ground librational state the probability of finding the hydrogen inside the cage decreases relatively slowly, for the highest librational state under study 90% of the hydrogen population exits directly, within several femtoseconds. For the doubly degenerate first excited librational state, direct exit amounts to 40%, the rest of the transient population decaying more slowly.

Figure 11 depicts the kinetic energy distributions of the outgoing hydrogen atoms. As discussed before, caging after photoexcitation from the ground librational state is very strong and, consequently, a dominant peak at zero hydrogen velocity is observed. For the degenerate first excited librational state we see a peak at zero velocity, as well as a well developed high energy peak corresponding to a free exit. The intense latter peak appears due to the fact that a significant fraction of the hydrogen probability is initially oriented sidewise with respect to the argon cluster, which prevents efficient caging. This trend is even stronger in the first nondegenerate excited librational state, where

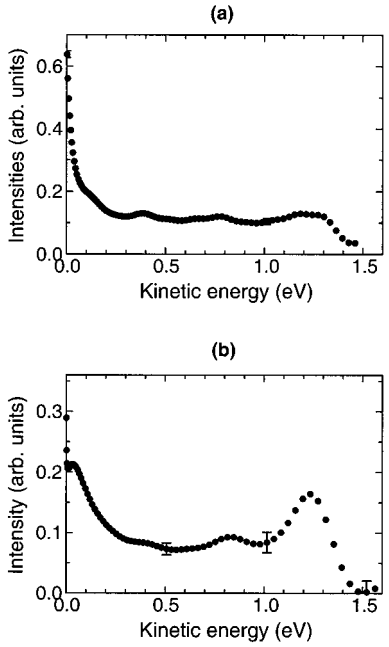

Figure 9. Experimental kinetic energy distributions of the photolyzed hydrogen for the (a) embedded and (b) surface isomers of $HBr(Ar)_n$ with a mean value of $\bar{n} = 115$.

most of the hydrogen probability points away from the argon atoms. As a result, high energy peaks, corresponding to a free hydrogen exit, predominate. In other words, caging can be efficiently "turned off" by a librational preexcitation. Such a librational preexcitation can be possibly realized experimentally either by an IR excitation of a combination band corresponding to HBr vibration (2650 cm^{-1})[22] and libration (typically 50−80 cm^{-1}) or simply by preparing the system under a higher temperature.

E. Classical vs Quantum Dynamics. In our previous studies[13,14] we have performed quantum dynamical simulations of HCl photodissociation in and on argon clusters corresponding to a vertical excitation by an infinitely short laser pulse. Similarly as other investigators,[3−6] we have evaluated the corresponding KED of the outgoing hydrogen as a Fourier transform of the hydrogen autocorrelation function. Here, we have performed an analogous quantum calculation for HBr photodissociation (considering only the $^1\Pi_1$ potential, which correlates with the ground state of Br) on the Ar_{12} cluster. The KED resulting from the quantum simulation is depicted in Figure 12; it is and compared to the results of classical Wigner trajectories calculations corresponding to a continuous photoexcitation at 243 and 193 nm.

We see that the quantum KED differs dramatically from the classical results, especially from that obtained for the 243 nm excitation. The main reason for this is not the difference between quantum and classical dynamics, but rather energetic considerations. The classical KEDs correspond to single wavelength excitations, either close to the maximum of HBr absorption for 193 nm, or at the low energy tail of the absorption spectrum for 243 nm. On the other hand, the infinitely short exciting pulse contains all wavelengths and the overall shape of the quantum KED is given by the reflection principle.[26] Understandably, the more energetic excitations either at 193 nm or by an ultrashort pulse lead to a stronger signal in KED corresponding to a nearly free hydrogen exit, while at lower excess energies for the 243 nm excitation peaking at zero velocity (i.e., caging) is more pronounced. Finally, we note that the 193 nm wavelength, which has been chosen for its experimental convenience, is shifted by 0.4 eV to the red from the peak of the absorption of the HBr molecule.[22] This is exactly the value by which the edge of the classical KED at 193 nm is shifted from the peak of the quantum distribution.

One quantum mechanical effect is the presence of a fine structure in the KED obtained using a quantum propagation (see Figure 12a). This structure is due to recurrences in the hydrogen wave function caused by reflections of the hydrogen flux from cage atoms and by interferences between the outgoing and reflected parts of the wave function. In other words, these are fingerprints of short-lived vibrational resonances due to caging.[13,14]

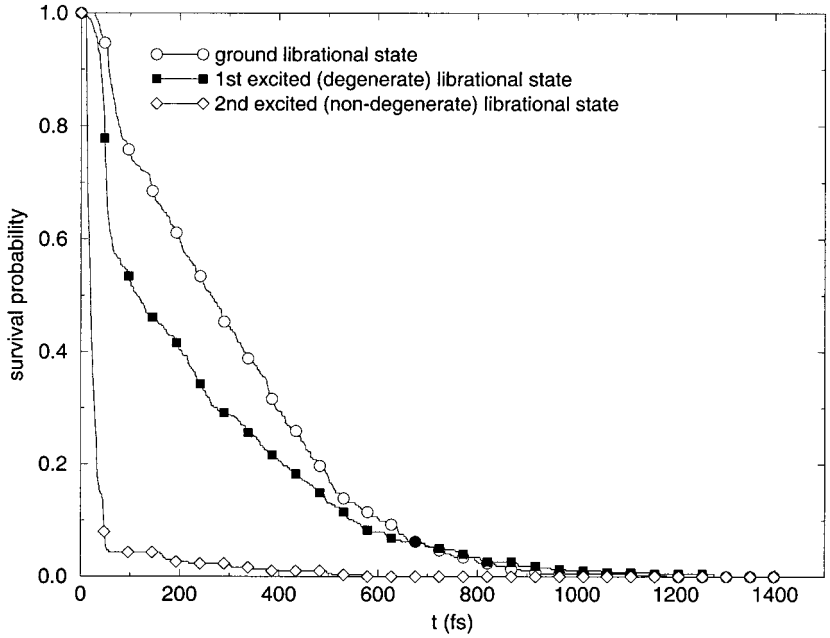

Figure 10. Transient probabilities of finding the photodissociating hydrogen inside the cluster for the surface solvated $HBr(Ar)_{146}$ cluster with HBr initially in the (a) ground, (b) first (degenerate) excited, and (c) first nondegenerate excited librational state.

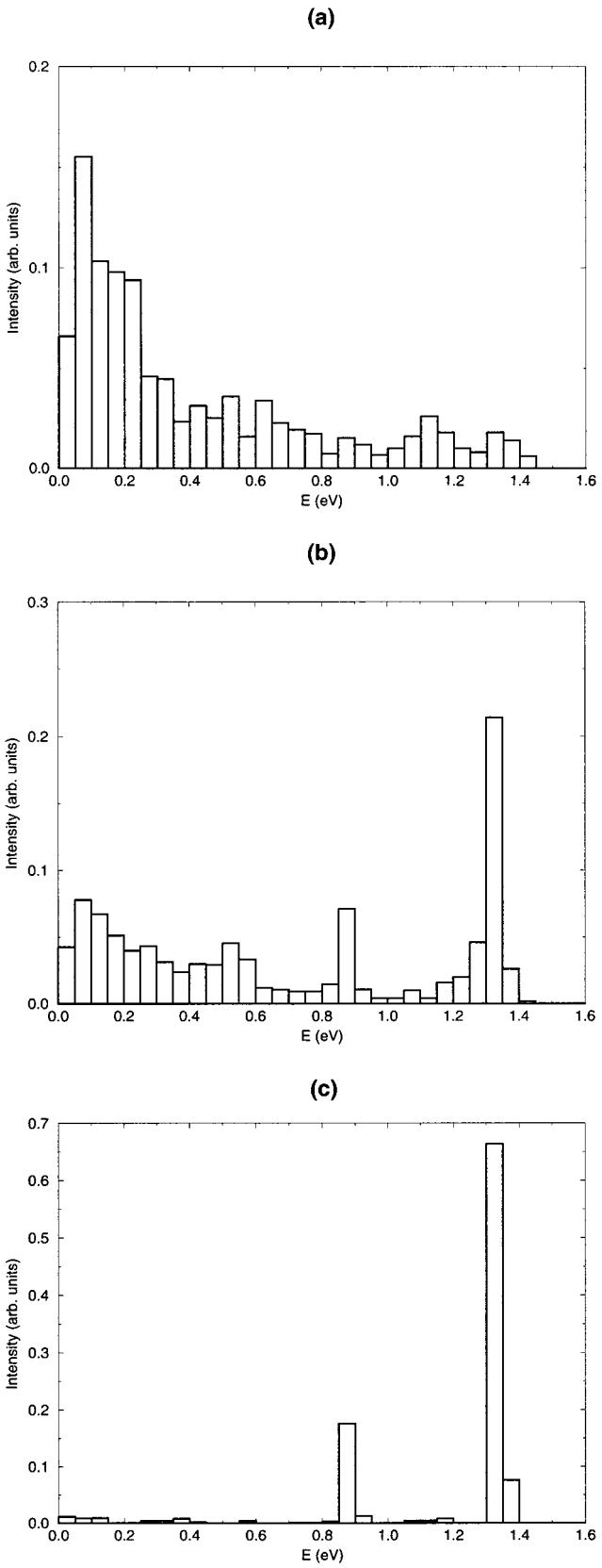

Figure 11. Final kinetic energy distributions of the photolyzed hydrogen for the surface solvated HBr(Ar)$_{146}$ cluster with HBr initially in the (a) ground, (b) first (degenerate) excited, and (c) first nondegenerate excited librational state.

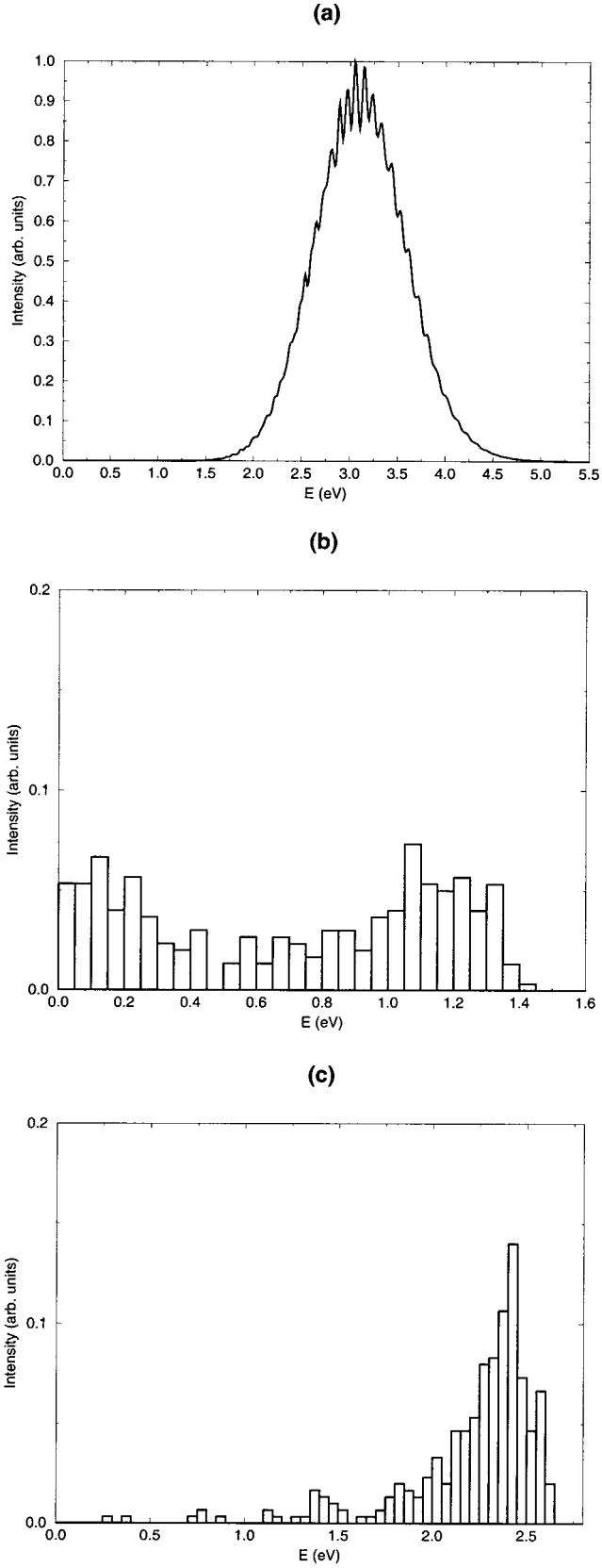

Figure 12. Final kinetic energy distributions of the photolyzed hydrogen for the embedded isomer of HBr(Ar)$_{12}$. (a) Quantum calculation for an infinitely short exciting pulse, (b) Wigner trajectories corresponding to the 243 nm excitation, and (c) Wigner trajectories for the 193 nm excitation.

VI. Conclusions

Molecular dynamics simulations and experiments have been performed for photodissociation of HBr absorbed at the surface or embedded inside large argon clusters. Calculations have been performed for 12, 54, 97, and 146 argon atoms, representing

one to three icosahedral solvation shells. It has been shown that the size effect is much stronger for embedded HBr, where a dramatic transition from weak to strong caging occurs between 54 and 97 argons. In contrast, starting from 54 argon atoms, caging is efficient for all surface structures and the size dependence is small. At the same time, for up to two argon solvation layers the cage effect is stronger for the surface compared to the embedded isomers. Near-quantitative agreement between the calculated and observed kinetic energy distributions of the outgoing hydrogen has been obtained. Calculations based on Wigner trajectories, which respect the initial quantum state of the system, have also demonstrated a novel approach to the control of the efficiency of caging. Namely, we show that the cage effect for surface solvated HBr can be turned off by a librational excitation prior to UV photolysis. Finally, different approaches to the calculation of kinetic energy distributions of the outgoing hydrogen, based either on quantum wave functions or on classical trajectories, are discussed and compared to each other.

Acknowledgment. We are grateful to Benny Gerber, Masha Niv, and Burkhard Schmidt for fruitful discussions. We also thank Brigitte Pouilly for providing us the potentials for excited HBr. Support from the Granting Agency of the Academy of Sciences via a grant No. B1010925 (to P.J.) and from the Deutsche Forschungsgemeinschaft within the SFB 357 (to U.B.) is gratefully acknowledged.

References and Notes

(1) Franck, J.; Rabinovitsch, E. *Trans. Faraday Soc.* **1934**, *30*, 120.
(2) Apkarian, V. A.; Schwentner, N. *Chem. Rev.* **1999**, *99*, 1481.
(3) Garcia-Vela, A. *J. Chem. Phys.* **1998**, *108*, 5755.
(4) Schroeder, T.; Schinke, R.; Mandziuk, M.; Bacic, Z. *J. Chem. Phys.* **1994**, *100*, 7239.
(5) Narevicius, E.; Neuhauser, D.; Korsch, H. J.; Moiseyev, N. *Chem. Phys. Lett.* **1997**, *276*, 250.
(6) Monnerville, M.; Pouilly, B. *Chem. Phys. Lett.* **1998**, *294*, 473.
(7) Garcia-Vela, A.; Gerber, R. B.; Buck, U. *J. Phys. Chem.* **1994**, *98*, 3518.
(8) Alimi, R.; Gerber, R. B. *Phys. Rev. Lett.* **1990**, *64*, 1453.
(9) Niv, M.; Krylov, A. I.; Gerber, R. B. *Faraday Discuss. Chem. Soc.* **1997**, *108*, 243.
(10) Niv, M.; Krylov, A. I.; Gerber, R. B.; Buck, U. *J. Chem. Phys.* **1999**, *110*, 11047.
(11) Baumfalk, R.; Nahler, N. H.; Buck, U.; Niv, M. Y.; Gerber, R. B. *J. Chem. Phys.*, in press.
(12) Schmidt, B. *Chem. Phys. Lett.* **1999**, *301*, 207.
(13) Zdanska, P.; Schmidt, B.; Jungwirth, P. *J. Chem. Phys.* **1999**, *110*, 6246.
(14) Zdanska, P.; Slavicek, P.; Jungwirth, P. *J. Chem. Phys.* submitted.
(15) Hillery, M.; O'Connel, R. F.; Scully, M. O.; Wigner, E. *Phys. Rep.* **1984**, *106*, 121.
(16) Baumfalk, R.; Buck, U.; Frischkorn, C.; Nahler, N. H.; Hüwel, L. *J. Chem. Phys.* **1999**, *111*, 2595.
(17) Hoare, M. R.; Pal, P. *Adv. Phys.* **1975**, *24*, 645.
(18) Raoult, B.; Farges, J.; de Feraudy, M. F.; Torchet, G. *Z. Phys.* **1989**, *12*, 85.
(19) Anderson, D. T.; Davis, S.; Nesbitt, D. J. *J. Chem. Phys.* **1997**, *107*, 1115.
(20) Hutson, J. M. *J. Chem. Phys.* **1989**, *91*, 4455.
(21) Aziz, R. A.; Slaman, M. J. *Mol. Phys.* **1986**, *58*, 679.
(22) Herzberg, G. Molecular Spectra and Molecular Structure; Van Nostrand: New York, 1950.
(23) Casavecchia, P.; He, G.; Sparks, R. K.; Lee, Y. T. *J. Chem. Phys.* **1981**, *75*, 710.
(24) Peoux, G.; Monnerville, M.; Duhoo, T.; Pouilly, B. *J. Chem. Phys.* **1997**, *107*, 70.
(25) Huang, Z.; Guo, H. *J. Chem. Phys.* **1992**, *96*, 8564.
(26) Schinke, R. Photodissociation Dynamics; Cambridge University Press: Cambridge, U.K., 1993.
(27) Jungwirth, P.; Gerber, R. B. *J. Chem. Phys.* **1995**, *102*, 6046.
(28) Feit, M. D.; Fleck, J. A.; Steiger, A. *J. Comput. Phys.* **1982**, *47*, 412.
(29) Buck, U.; Galonska, R.; Kim, H.-J.; Lohbrandt, P.; Lauenstein, C.; Schmidt, M. In *Atomic and Molecular Beams. The State of the Art 2000*; Campargue, R., Ed.; Springer: Berlin, 2000.
(30) Baumfalk, R.; Buck, U.; Frischkorn, C.; Gandhi, S. R.; Lauenstein, C. *Ber. Bunsen-Ges. Phys. Chem.* **1997**, *101*, 606.
(31) Buck, U.; Krohne, R. *J. Chem. Phys.* **1996**, *105*, 5408.
(32) Wales, D. J.; Doye, J. P. K. *J. Phys. Chem. A* **1997**, *101*, 5111.
(33) Baumfalk, R. Ph.D. Thesis, Gottingen, 1999.
(34) Jungwirth, P. *Chem. Phys. Lett.* **1998**, *289*, 324.
(35) Jungwirth, P.; Zdanska, P.; Schmidt, B. *J. Phys. Chem. A* **1998**, *102*, 7241.